

# Towards a continuous microfluidic rheometer

Pierre Guillot\*, Thomas Moulin, Matthieu Guirardel, Arash Dodge, Mathieu Joanicot, and Annie Colin  
*Rhodia Laboratoire du Futur, Unité mixte Rhodia-CNRS, Université Bordeaux I,  
UMR 5258, 178 Avenue du Docteur Schweitzer, 33608 Pessac, FRANCE*

Charles-Henri Bruneau and Thierry Colin  
*MAB Université Bordeaux1, CNRS UMR 5466, INRIA Futurs projet MC2,  
351 cours de la libération, 33405 Talence, FRANCE*

(Dated: October 23, 2007)

In a previous paper we presented a way to measure the rheological properties of complex fluids on a microfluidic chip [1]. The principle of our method is to use parallel flows between two immiscible fluids as a pressure sensor. In fact, in a such flow, both fluids flow side by side and the size occupied by each fluid stream depends only on both flow rates and on both viscosities. We use this property to measure the viscosity of one fluid knowing the viscosity of the other one, both flow rates and the relative size of both streams in a cross section. We showed that using a less viscous fluid as a reference fluid allows to define a mean shear rate with a low standart deviation in the other fluid. This method allows us to measure the flow curve of a fluid with less than 250  $\mu\text{L}$  of fluid. In this paper we implement this principle in a fully automated set up which controls the flow rate, analyzes the picture and calculates the mean shear rate and the viscosity of the studied fluid. We present results obtained for Newtonian fluids and complex fluids using this set up and we compare our data with cone and plate rheometer measurements. By adding a mixing stage in the fluidic network we show how this set up can be used to characterize in a continuous way the evolution of the rheological properties as a function of the formulation composition. We illustrate this by measuring the rheological curve of four formulations of polyethylene oxide solution with only 1.3 mL of concentrated polyethylene oxide solution. This method could be very useful in screening processes where the viscosity range and the behavior of the fluid to an applied stress must be evaluated.

Keywords: Microfluidics, Rheology, Complex Fluids

## INTRODUCTION

Combinatorial chemistry has opened new paths for synthesizing large libraries of novel materials and formulations. High throughput characterization techniques become essential in order to benefit from these new synthesis methods. In fact, a systematic investigation of the relevant properties is required to select the convenient formulation or material. In this paper, we present a set up which allows to perform continuous rheological measurements on a microfluidic chip. Rheology is the study of the deformation and flow of a material in response to an applied stress. For simple liquids, the shear stress is linearly related to the shear rate via the viscosity coefficient. This is not always the case. In complex fluids, the existence of a mesoscopic length scale ranging between the molecular size and the whole sample [2] may induce coupling between the structure of the fluid and the flow leading to a non-Newtonian behavior. Characterizing the response of a sample under flow requires thus the establishment of a rheological curve giving the evolution of the viscosity as a function of the applied shear rate. Rheological characteristics of fluids are es-

sential properties in many fields. For example in paint industries, the viscosity of the paint must be low enough under high shear rates in order to coat the surface well, but must be high enough under low shear conditions to stay on the brush. High viscosity in formulations is often used to stabilize an emulsion or a suspension in the food and personal care industries. Adjusting the viscosity of a formulation to the required range involves a long series of trials and tests. Microfluidics, which deals with methods and materials to control and handle liquid flows on length scales ranging from tens to hundreds of micrometers, offers numerous prospects along these lines to formulate and characterize products [3]. This is the lab on a chip concept. In fact, adding a mixing step before a characterization one at the submillimetric length scale allows to use very small volumes of fluid to screen different formulations in a continuous way. The easiest type of rheometer to miniaturize, allowing for a continuous approach, are capillary rheometers. In such a rheometer, the principle is to establish the relationship between the pressure drop and the flow rate of a fluid flowing through a capillary that has a constant cross-section.

On-line capillary rheometers have been used for over 30 years in polymer and food engineering [4–9]. Devices with features on the sub-millimeter length scale appeared in the last 10 years. Using pressure-driven flows, Weng et al. have developed a viscosimeter with a thermostat

---

\*Corresponding author: pierre.guillot@eu.rhodia.com

[10]. They measured the pressure drop and the flow rate of a liquid passing through a microtube of 20 microns of diameter. Using 60 microliters of sample, they achieved accurate viscosity measurements with a precision of less than 5% at different temperatures. However, in their approach they only measured low viscosity (less than  $10^{-2}$  Pa·s) of Newtonian fluids without calculating the shear rate. Kang and coworkers [11] measured the total pressure drop along a microchannel for an imposed flow rate using a pressure sensor. They measured the rheological properties of polymer solutions at high shear rates. The main drawback of their technique is that their system relies on the use of an external pressure transducer, which measures the sum of the true microchannel pressure drop plus those due to entrance and exit effects. To take these effects into account, both complex calibrations and corrections, which required to perform experiments in channels of various lengths and cross-sections, have to be applied. Moreover, the use of an external transducer may result in a delay time quite long for the response of the rheometer when the flow rate becomes low [12].

To avoid these corrections and delay times, Galambos and coworkers [13] have proposed to use the features of specific microfluidics flows. After a T junction, two miscible fluids flowing side by side in the outlet channel are mixed by interdiffusion. Right after the T junction, the interface between the two fluids is still sharp since, in their experimental conditions, diffusion is slower than convection. In the channel, the position of the interface is fixed by the ratio of the flow rates of the two fluids and by the ratio of their viscosities. These authors show that by measuring the position of this interface using fluorescence microscopy, they manage to compute the viscosity of one sample by knowing the flow rates and the viscosity of the other fluid. This elegant method, which does not require the implementation of a sensor on or outside the microdevice, allows to measure the pressure drop of the flow.

Using two immiscible fluids, we used this approach to measure the pressure drop of the flow and extend it to complex fluid. The mean shear rate and the viscosity of the studied fluid are then defined applying classical rheological procedures. The flow curve of the sample is calculated by performing measurements at different flow rates [1]. This method seems well suited to characterize the flow properties of a sample with a few quantity of it. This could be very helpful in screening processes where various formulations are prepared and need to be evaluated. In this paper we implement our method in a set up engineered to perform continuously measurement in an automated fashion. In the first part we recall the principle of the method used to determine the fluid flow curve. We then present the routine developed to analyze the image and explain the main structure of our program. We finally show the results that we obtained with measurements on a single sample and continuous measurements

of various formulations prepared on-chip.

## PRINCIPLE OF THE MICRORHEOMETER

Following the works of Galambos [13] and Groisman [14, 15], we measure the pressure drop in a microchannel using optical microscopy. In this section we describe our method to measure pressure drop in a parallel flow. More details can be found elsewhere [1]. Our microdevices are T channel (see Fig. 1) made in glass polydimethylsiloxane (PDMS) by using soft lithography technology [16]. When two immiscible fluids are injected, various flows such as droplets, pearl necklaces, disordered patterns or parallel flows can be obtained after the junction [3, 17–20]. However, in a wide range of flow rates, the two immiscible fluids flow side by side forming a laminar parallel flow. The range of flow rates can be greatly increased by using a rectangular channel instead of a square one [19]. Therefore, all our experiments are performed in  $200\ \mu\text{m} \times 100\ \mu\text{m}$  microchannels. In the following we recall the mean properties of the parallel flow.

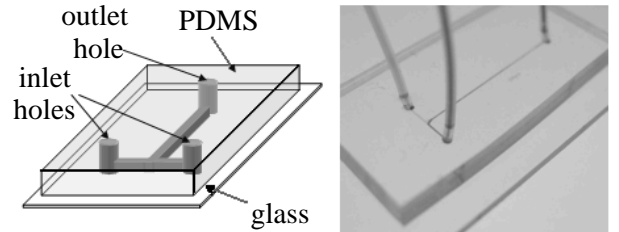


FIG. 1: Sketch and picture of our microfluidic devices.

### Properties of the parallel flow

The shape of the parallel flow in a glass PDMS channel is ruled by wetting and injection conditions. The mean features of this shape can be studied using confocal fluorescence microscopy [21, 22]. To do so, a small amount of rhodamine 6G is added in the aqueous phase which is a mixture of water and glycerine adjusted to match the refractive index with the one of the hexadecane. A typical cross-sectional image is presented in the Fig. 2. The walls of the  $200\ \mu\text{m} \times 100\ \mu\text{m}$  microchannel have been drawn to the picture. The contact angle on the PDMS and on the glass are different due to the differences in affinity between the oil and the two solid plates (PDMS or glass). The free fluid-fluid interface has a curvature with a constant radius. This shape implies that the pressure jump across the interface is constant. This point is important because to obtain an unidirectional flow the pressure in a cross section has to be constant in both fluids, *i.e.* the

pressure jump at the interface must be the same all along the interface. The one radius shape is thus a signature of an unidirectional flow. We can also notice that the gravity does not affect the free fluid-fluid interface as it is expected in these dimensions that are much lower than the capillary length. Knowing that curvature, it is possible to determine this interface shape from transmission picture. In fact, by adjusting the contrast of the picture, mismatched lines appear; this reveals the characteristic lines and fully describes the shape as shown in Fig. 2. In fact, the mismatched lines correspond to the PDMS walls (W), to the interface position (I) and to the contact lines on the glass slide ( $C_g$ ) or on the PDMS surface ( $C_p$ ). Assuming that the interface is circular, the knowledge of the position of these lines allows us to calculate the radius of the interface and the position of its center. Hereafter, we design the fluid with a convex shape the inner fluid whereas the other fluid is called the outer fluid.

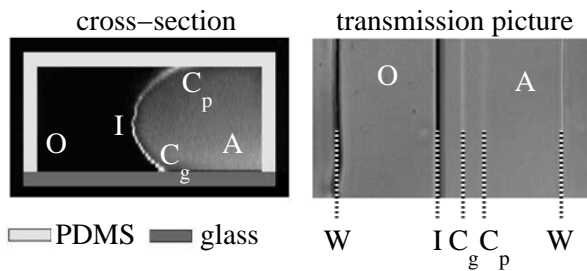


FIG. 2: Cross-section and transmission pictures of a parallel flow between hexadecane (O) and an aqueous phase with rhodamine (A) in a  $200 \mu\text{m} \times 100 \mu\text{m}$  microchannel. The interface between the two fluids is circular. Mismatched lines on transmission pictures correspond to the characteristic lines of the shape.

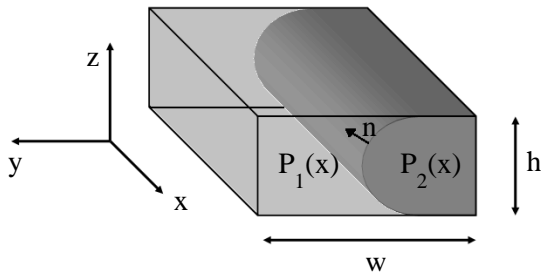


FIG. 3: Notations used.

In a steady state, the flow field for incompressible Newtonian fluids is obtained by solving the Stokes equation for both fluids:

$$\eta_i \Delta \vec{v}_i = \text{grad} P_i \quad (1)$$

where  $\vec{v}_i$ ,  $\eta_i$  and  $P_i$  are the velocity vector, the viscosity

and the pressure inside the fluid  $i$ . In our notations,  $i$  equals 1 for the outer fluid and  $i$  equals 2 for the inner one. In a parallel flow the flow is unidirectional. With the notations of the Fig. 3, the velocity vector has only one component in the  $x$  direction. This implies that the pressure in each fluid is only a function of  $x$ . The pressures in both fluid are linked by the Laplace law through:

$$P_2(x) - P_1(x) = \frac{\gamma}{R(x)} \quad (2)$$

where  $\gamma$  is the surface tension and  $R(x)$  is the radius of the interface. As  $R(x)$  is constant all along the channel the pressure gradient in both fluids are equal:

$$\frac{\partial P_1}{\partial x} = \frac{\partial P_2}{\partial x} \quad (3)$$

This set of equations is closed by defining the boundary conditions, namely: the velocity and the tangential components of the stress tensor are continuous at the interface and there is no slip at the walls for both fluids [23, 24]. Note that the viscous surface term is neglected in the shear stress tensor [1].

The resolution of the equation 1 for given flow conditions (channel dimension, interface shape, pressure gradient and viscosities) allows to calculate the flow field. The flow rate  $Q_1$  and  $Q_2$  of both fluids are then calculated by integrating the flow field according to:

$$Q_i = \int_0^w \int_0^h u_i(y, z) dy dz \quad (4)$$

where  $w$  is the width of the channel and  $h$  is the height. The mean shear rate in each fluid  $\dot{\gamma}_i$  and its standard deviation can be estimated by:

$$\dot{\gamma}_i = \frac{1}{\Sigma_i} \int_0^w \int_0^h \sqrt{\left(\frac{\partial u_i}{\partial y}\right)^2 + \left(\frac{\partial u_i}{\partial z}\right)^2} dy dz \quad (5)$$

$$\Delta \dot{\gamma}_i = \frac{1}{\Sigma_i} \int_0^w \int_0^h \sqrt{\left(\frac{\partial u_i}{\partial y}\right)^2 + \left(\frac{\partial u_i}{\partial z}\right)^2} - \dot{\gamma}_i^2 dy dz \quad (6)$$

where  $\Sigma_i$  is the cross-sectional surface filled with the sample  $i$ .

A dimensional analysis of this set of equations points out that the relative space occupied by each fluids in a cross section of the channel is directly related to their viscosity and flow rate ratios. This is well illustrated by Fig. 4 and Fig. 5. Increasing the aqueous flow rate by keeping the oil flow rate constant leads to the enlargement of the aqueous stream width (see Fig. 4). As shown in Fig. 5, the position of the interface between two Newtonian fluids (*i.e.* with constant viscosity ratio) does not move when the flow rates are changed while the ratio between them is kept constant.

Therefore, measuring the geometrical features of the flow, knowing both flow rates and one of the two viscosities allows us to obtain the other viscosity. The pressure

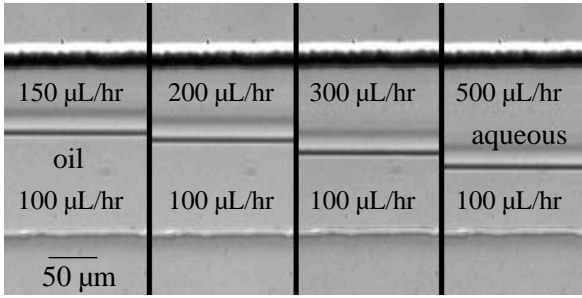


FIG. 4: Optical pictures of the parallel flow taken for various flow rate ratios in a  $200 \mu\text{m} \times 100 \mu\text{m}$  microchannel. The oil phase is hexadecane. The aqueous phase is a solution of Sodium dodecyl sulfate (SDS) in water at the critical micellar concentration (cmc) and is located in the upper part of the figure. The flow rates of water and hexadecane are specified on the picture. Note that the interface between the two fluids moves towards the lower part when the water flow rate is increased.

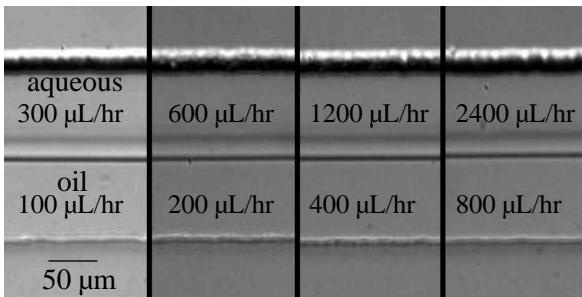


FIG. 5: Optical pictures of the parallel flow taken for a fixed ratio between the flow rates in a  $200 \mu\text{m} \times 100 \mu\text{m}$  microchannel. The oil phase is hexadecane. The aqueous phase is a solution of water with SDS at the cmc and is located in the upper part of the figure. The flow rates of water and hexadecane are specified on the figure. The interface between the two fluids does not move for the different flow rates.

drop in the channel can be then deduced from the absolute value of the flow rate. However, due to the shape of the interface there is no analytical solutions of the flow field and numerical procedures are required to perform the calculation.

#### Definition of the viscosity and shear rate for complex fluids

The details of the procedure use in the numerical simulations are described in [1]. A finite volume discretization of the equations that ensures the continuity of the fluxes at the interface [25] is used on a cartesian mesh. We are able to compute the flow rate of both fluids assuming

them to be Newtonian. However, in our experiments, we impose the two flow rates, we measure the position and the shape of the interface, and we only know the viscosity of one of the two fluids. Therefore, we need to solve the inverse problem to find the viscosity ratio leading to the measured interface shape for the imposed flow rate ratio. To do so, we calculate the flow rate ratio  $Q_1/Q_2$  obtained for an arbitrary viscosity ratio  $\eta_1/\eta_2$  and compare it to the experimental one. We converge towards the experimental flow rate ratio by adjusting the viscosity ratio through numerical methods. We use the fact that, for a given position of the interface and a given flow rate ratio, there exists only one viscosity ratio that solves the Stokes equation (see Fig. 6). The mean shear rate  $\dot{\gamma}$  sustained by the fluid is then calculated by differentiating the velocity field using equation 5.

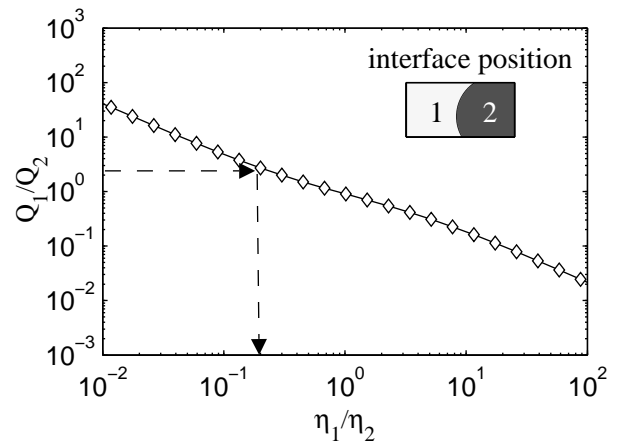


FIG. 6: Flow rate ratio  $Q_1/Q_2$  as a function of the viscosity ratio  $\eta_1/\eta_2$  for a given position of the interface. The channel dimensions are  $200 \mu\text{m} \times 100 \mu\text{m}$ . The knowledge of the flow rate ratio allows to determine the viscosity ratio.

These definitions are only true for Newtonian fluids. To define the viscosity and the shear rate of a complex fluid we use a procedure widely used in rheology. We associate to the non-Newtonian fluid the viscosity and the mean shear rate that a Newtonian fluid would have under the same experimental conditions (same flow rates and same viscosity of the standard fluid). This approximation can be used when the shear stress in the sample is the most homogeneous possible. The Fig. 7 represents the homogeneity of the fluid 2 shear rate for three viscosity ratios. It appears that the shear rate of the fluid 2 is defined with less than 15% of error when the fluid 1 is ten times less viscous and for a flow rate ratio  $Q_1/Q_2$  between 10 and 100. In this case the flow profile of the unknown fluid looks like a shear flow as depicted in Fig. 8. In our experience we will thus use a reference fluid less viscous. To calculate the error bars we take into account the standard deviation of the shear rate value and we

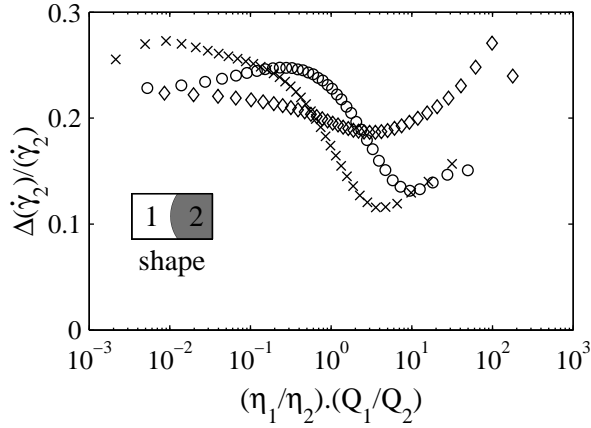


FIG. 7: Standard deviation of the mean shear rate of fluid 2 divided by the mean shear rate as a function of  $(Q_1/Q_2)(\eta_1/\eta_2)$ . Microchannel dimension is  $200 \mu\text{m} \times 100 \mu\text{m}$ . This deviation is calculated for different viscosity ratios  $\eta_1/\eta_2$ . ( $\times$ ) corresponds to a ratio of 0.1, ( $\circ$ ) to a ratio of 1 and ( $\square$ ) to a ratio of 10.

calculate the error made on the viscosity ratio assuming an error of  $\pm 5 \mu\text{m}$  on the detection of the position lines (see details in [1]).

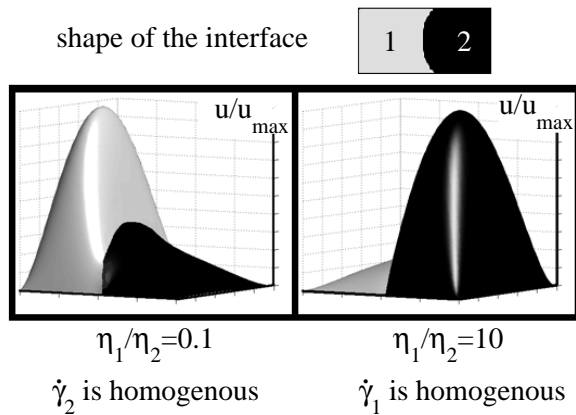


FIG. 8: Flow profile in a  $200 \mu\text{m} \times 100 \mu\text{m}$  channel as a function of the viscosity ratio  $\eta_1/\eta_2$ . The mean shear rate  $\dot{\gamma}$  is well defined when the reference fluid used to form a parallel flow is less viscous.

## AUTOMATION AND ANALYSIS

The purpose of this paper is to implement our method and our analysis in an automated set up. Therefore, each operation accomplished by an operator during an experiment must be automated. When an experiment is performed we need to execute the following tasks: changing

the flow rates, analyzing the picture, extracting the correct lines and calculating the viscosity and the shear rate. The syringe pumps control is straight forward and can be easily done via the RS232 by using the code given by the supplier [26] and the Matlab software. The numerical calculation of the viscosity and shear rate are also done with Matlab and has already been developed [1]. For each flow rate it is necessary to take a picture of the flow and analyze it. To take the picture at a given frame rate we use a CCD camera connected to an acquisition card controlled by the LabView software. The main difficulty remains in finding a way to robustly analyze the picture in order to extract the characteristic lines introduced in the Fig. 2. In the following we described the way that we use to perform this analysis.

The first issue is that, to identify all the lines on a picture, it is necessary to finely adjust the focus and the contrast of the microscope. When manual experiments are performed these settings are often readjusted to obtain pictures which contain all the lines ( $C_p$ ,  $C_g$  and I). Without operator, it is not possible to change the setting during the experiment. Since sometimes all the lines do not appear on the same picture, it is necessary to define a rule which can be applied on every pictures. The most difficult lines to distinguish are  $C_p$  or  $C_g$  because they are quite close and less contrasted than the other ones. However, due to the fact that they are close, it is tempting to make the approximation that they are confounded. Doing this, we limit our detection to four characteristic lines. Before going further, it is important to quantify the error made doing this approximation on the determination of the shape. To estimate the maximum error we calculate the viscosity ratio  $(\eta_1/\eta_2)_{C_p}$  when the detected line is  $C_p$  and  $(\eta_1/\eta_2)_{C_g}$  when  $C_g$  is detected. The difference between the viscosity ratio found with the approximate shape and the one found with the true shape allows to estimate the mean error made with this approximation through:

$$\Delta_R(\eta_1/\eta_2) = \frac{\eta_1/\eta_2 - (\eta_1/\eta_2)_{C_p}}{2\eta_1/\eta_2} + \frac{\eta_1/\eta_2 - (\eta_1/\eta_2)_{C_g}}{2\eta_1/\eta_2} \quad (7)$$

This leads to a small error in determining the viscosity ratio as shown in Fig. 9 where  $\Delta_R(\eta_1/\eta_2)$  is plotted as a function of  $Q_1/Q_2$ . The shape considered is put in insert. This a  $200 \mu\text{m}$  radius circle centered at  $y=-100 \mu\text{m}$  and at  $z=30 \mu\text{m}$  with the notation of Fig. 3 and an origin in the right bottom corner. Note that this flow geometry is realistic and corresponds to a case with a high asymmetry of the wetting angle on the PDMS and on the glass surfaces. The error on viscosity ratio made with the approximation on the shape is lower than the one due to experimental uncertainties (10-20 %) discussed in [1]. Therefore we will not take this error into account in the calculation of the error bars.

The identification of the lines on the images are

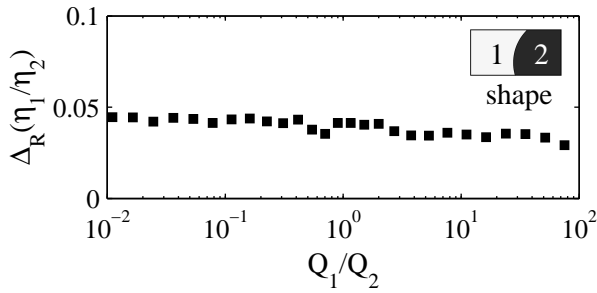


FIG. 9: Error on the viscosity ratio due to the approximation of the shape.  $\Delta_R(\eta_1/\eta_2)$  is the relative error between the viscosity ratio found with the real shape and the one with the approximate shape.

processed using a Matlab routine. The lines are detected using Hough Transform (HT), a method first proposed by P. Hough in 1962 [27, 28]. The HT can only be applied on black and white pictures. Thus, the use of the HT requires that we transform our initial picture into a black and white picture where the lines clearly appear. Using an edge detection step allows us to identify and keep the strong intensity gradient regions which naturally include the lines. The picture obtained after this step is not yet black and white and it is thus necessary to threshold it before applying the HT. By trying various filters, it appears that the critical step of this method is the edge detection. It is very important to obtain a low noise picture keeping mainly the lines. The Sobel filter gives the best and more robust edge detection results, but only detects the gradient in the vertical and horizontal directions. This constrains us to rotate the initial picture in order to obtain horizontal or vertical walls. We arbitrarily chose the horizontal orientation. The analysis of the picture can be thus decomposed in two stages, a rotation step following by a detection step.

To rotate the picture in order to orient the walls along the horizontal direction we follow the procedure shown in Fig. 10. The initial image (see Fig. 10-a)) is filtered using the Canny filter and is transformed into a black and white picture (see Fig. 10-b)) to apply a first HT. Canny filter has the advantage that it does not prefer any direction in space and is a good compromise between edge detection and noise. The HT is then applied to this picture. In this step we do not search all of the characteristic lines but we look at the longest lines to find the orientation of the walls with respect to the horizontal line. Detected lines are added to the initial picture (see Fig. 10-c)). The image is then rotated by the measured angle value so that it appears horizontal. To identify fluids by their position (upper or lower side), we perform a function check by asking to the operator at the beginning of the routine if the upper phase in the figure corresponds to the inner fluid. With this information, we obtain a horizontal

picture where the inner phase is on the upper side of the picture (see Fig. 10-d)).

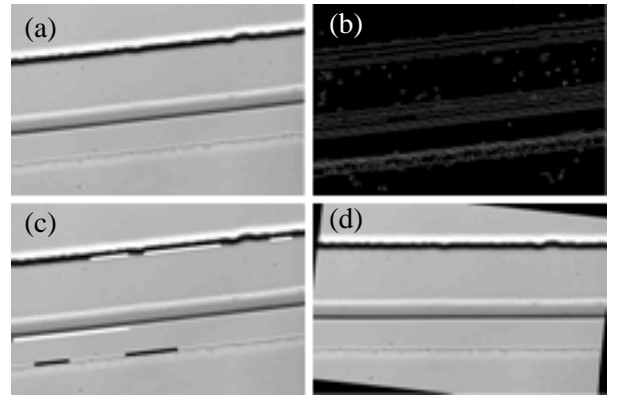


FIG. 10: Rotation process of the picture. a) initial picture b) black and white picture obtained after thresholding the Canny filtered image c) the longest detected lines through the Hough transform are added to the picture d) rotated picture.

The rotated picture is then used to perform the complete analysis of the lines as depicted in Fig. 11. The image is filtered with a Sobel filter (see Fig. 11-b)). This allows a very good precision in the edge detection but generates a poorly contrasted image. The contrast is enhanced by increasing the value of each pixel in the picture by a power of 3 (see Fig. 11-c)). After the contrast improvement, the image is thresholded to obtain a black and white picture (see Fig. 11-d)). The HT is then applied to this black and white image. We only focus on the horizontal lines since we know that all the lines of interest are horizontal.

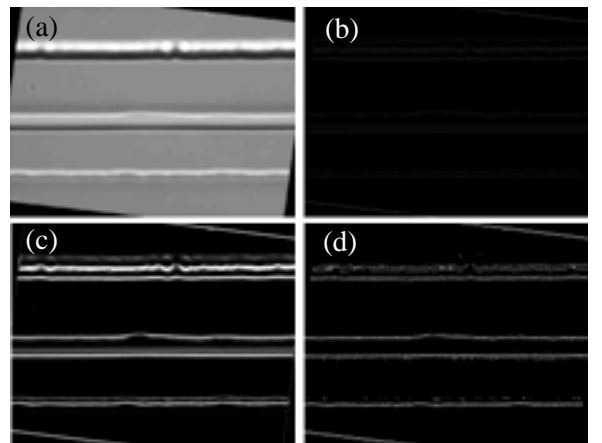


FIG. 11: Detection of the lines. a) rotated picture b) Sobel filtered picture c) amplification of the contrast d) black and white picture in which the Hough transform is applied.

The HT gives the mean length of all horizontal lines as

a function of the vertical position. This histogram allows us to choose different lines (see Fig. 12). In this figure we can clearly identify groups of lines. Line positions are chosen at an average position for each group of lines. In order to not detect the same line two times, a minimum distance between each line is set. These minimum distances have been chosen through our own experience. We do not take into account flows where one of the fluids occupies most of the channel volume. We also avoid having contact lines that are too close to the interface because we never saw straight interfaces for parallel flows in our geometry. Thus, C and I must be separated of 5 % of the channel width ( $10 \mu\text{m}$ ) and should not be placed closer than 13 % of the channel width ( $15 \mu\text{m}$ ) from the walls.

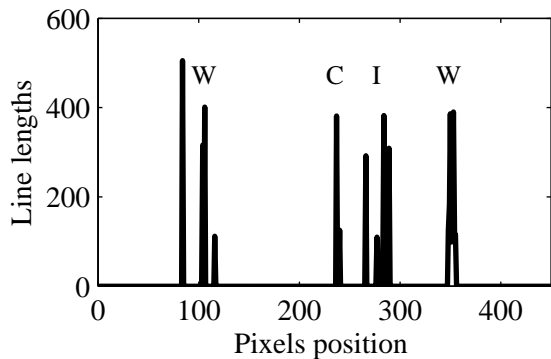


FIG. 12: Line lengths as a function of the vertical position. This histogram gives the position of the contact line, the interface and the walls.

The lines detected through this procedure are added to the rotated picture (see Fig. 13) and the picture is saved with the detected lines on it. This can be useful to check for outlier points at the end of an experiment.

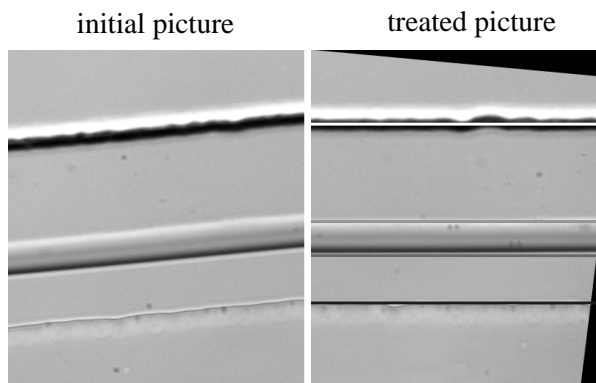


FIG. 13: Picture taken from an experiment and picture after performing the image analysis. Detected lines are added to the final picture.

## METHODS AND SET UP

### Set up

Our microfluidic devices are fabricated using soft lithography [16]. A mold is obtained by patterning photoresist (Su-8 series, Microchem) on a silicon wafer by standard photolithography. PDMS (Sylgard 184, Dow Corning) is cast on the mold and cured at  $65^\circ\text{C}$  for one hour. The channels are sealed to a glass plate after an oxidation step in an UV cleaner (Jelight). Thus, the microchannels have three walls made from PDMS and one that is glass. Channel dimensions are measured with a profilometer (Dektak 6M, Veeco). The microdevices used in our experiments have two inlet arms which meet at a T junction with a funnel design. The use of a funnel allows us to reduce the droplet formation domain.

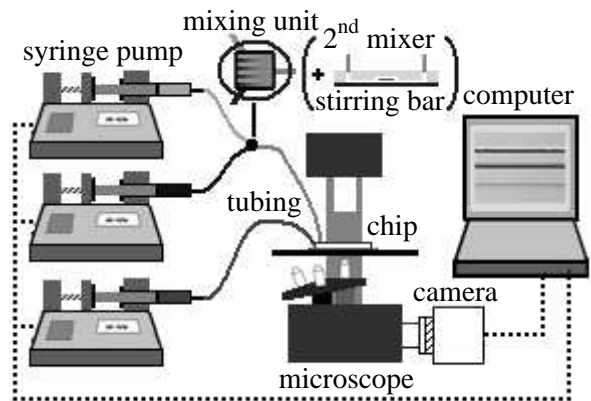


FIG. 14: Set up used in our experiments. This set up allows continuous measurements on the chip. Syringe pumps are controlled by the computer. Two syringe pumps inject the two fluids which are mixed before the microfluidic chip. A third pump injects the reference fluid to form a parallel flow in the channel. Observations are done with an optical microscope and pictures are recorded with a CCD camera at a given frame rate.

The inlet channels are connected via tubing to syringes loaded with the fluids. Syringe pumps (PHD 2000, Harvard apparatus) allow us to control the flow rates of the liquids between  $1 \mu\text{L/hr}$  and  $60 \text{ mL/hr}$  (see Fig. 14). The syringe pumps are controlled with a Matlab routine via the RS232 interface [26]. Images are taken with a CCD camera (FK-7512-IQ Cohu, Pieper GmbH) that is connected to an acquisition card (PCI 1407, National Instruments). A home made image acquisition program allows us to take pictures at a given frame rate. When three fluids are used, a mixing device (SIMM-V2, IMM) is added before the chip to increase the efficiency of the mixing [29]. This device divides the two fluid streams into multiple streams and recombines them in order to increase the contact surface between the two fluids. As

mixing in a microchannel is only a diffusive process, the mixing time is greatly reduced by increasing the interface between the two fluids. This device is placed as close as possible to the microfluidic chip in order to reduce the dead volume. Between samples, we flush the previous sample by increasing the flow rates during two equilibrium times. This ensures that the fluid passes through the dead volume. When this set up is not efficient enough to obtain a good mixing of the fluids, a mixing chamber is added between the IMM mixer and the microfluidic chip similar to the one proposed by Wu and coworkers [30]. This chamber consists in a 1.5 mm high cylinder with a radius of 4 mm in which a stirring bar is included before sealing. Inlet and outlet channels are lower than the height of the stirring bar. The device is made from PDMS and glass. Note that the dead volume is increased in comparison with the previous mixing network. More liquid is therefore able to flush the system between two different compositions.

To compare our measurements with classical ones, we performed rheological measurements on our solutions in a cone and plate rheometer (AR-G2, TA instruments) with a 4 cm diameter and  $2^\circ$  angle cone cell.

### Procedure

To carry out an experiment, we first fill our fluidic network to obtain a steady flow on the microfluidic chip. At the beginning of the experiment a checkby function ask where is the reference fluid and the value of its viscosity. A file with all the flow rate is then loaded by the program and the experiment starts. The image acquisition software records picture at a given frame rate in an acquisition folder. The Matlab routine controls syringe pumps and analyzes the picture. As soon as a picture is recorded the flow rate are changed, the picture is analyzed and the viscosity and the shear rate are calculated. It does it until it reaches the end of the flow rate file. At the end of the experiment we obtained a file which contains the viscosity, the shear rate and the other experimental parameters. When formulations are prepared on the microfluidic network the flow rates of the miscible fluids are chosen to obtain the targeted compositions. All these values are reported in the file which is loaded at the beginning of the experiment. Between two different compositions, the fluidic network is flushed by injecting twice the dead volume of the new composition.

### Materials

In this work various simple and complex fluids have been used. The Newtonian fluids are silicone oils of different viscosities, glycerine and dilute solutions of Sodium Dodecyl Sulfate (SDS) above the critical micellar concen-

tration (cmc) in water (cmc =0.24 wt %). Various non-Newtonian solutions have been studied; these are dilute solutions of polymers and surfactants in water. Dilute solutions of polymers are PolyEthyleneOxide (PEO) with a molecular weight of 4,000,000 (4M) at 2 wt % and 4 wt % in water. The first surfactant solution is a mixture made of CetylTrimethylAmmonium Bromide (CTAB) diluted at 0.05 mol/L in a solution of sodium salicylate (NaSal) at 0.02 mol/L in water. The second one is as a mixture made of CetylPyridinium Chloride (CpCl) and NaSal diluted at 6 wt % in a solution of NaCl at 0.5 mol/L in water. This system is known to form wormlike micelles [31, 32].

## RESULTS

In this section we present our results obtained on Newtonian and non-Newtonian fluids with our automated microfluidic set up. Error bars on viscosity and on shear rate are calculated as previously discussed and are plotted with a cross which relative size depends on the calculated error for the two values. Results are compared with classical measurements.

### Simple measurement

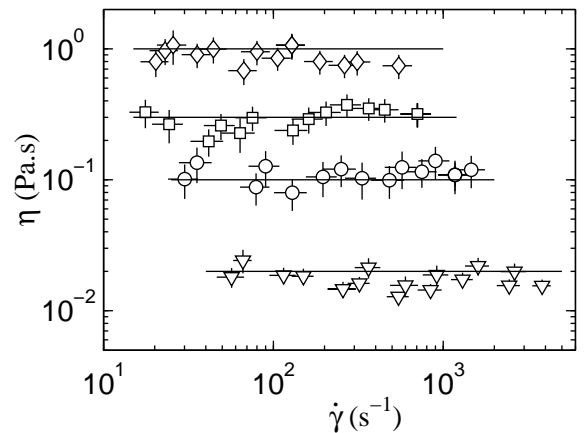


FIG. 15: Viscosity as a function of shear rate for four different silicone oils. Viscosity is constant with the shear rate.  $\nabla$ ,  $\circ$ ,  $\square$  and  $\diamond$  are results obtained with our microrheometer for the 20 mPa.s, 100 mPa.s, 300 mPa.s and 1000 mPa.s oils, lines are the data given by the supplier. Crosses behind symbols correspond to the calculated error bars on the shear rate and the viscosity.

Figure 15 presents the viscosity measurements with error bars obtained on different silicone oils of 20, 100, 300 and 1000 mPa.s. The measurements are performed at  $22^\circ\text{C}$ . The viscosities found for the different oils are in



quite good agreement with the values given by the supplier. Figure 16 presents the rheological curve obtained on PEO at 2 wt % in water. Results and error bars obtained with our set up are in good agreement with results obtained on a classical rheometer. During this experiment we used less than 350  $\mu\text{L}$  of PEO solution in the microfluidic chip.

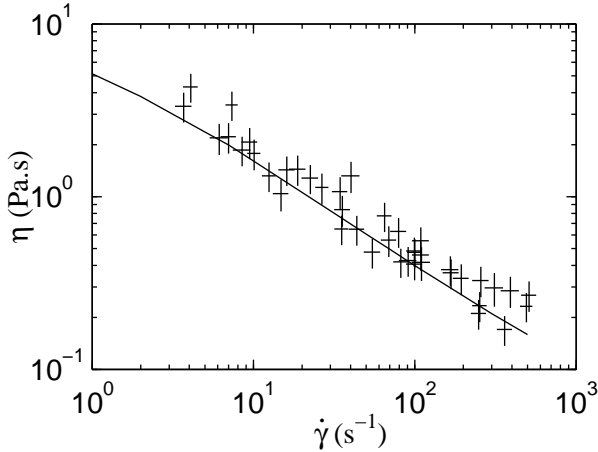


FIG. 16: Viscosity as a function of shear rate for a solution of PEO at 2 wt % in water. + are results and error bars obtained with our microrheometer and line is the one obtained with a cone and plate rheometer.

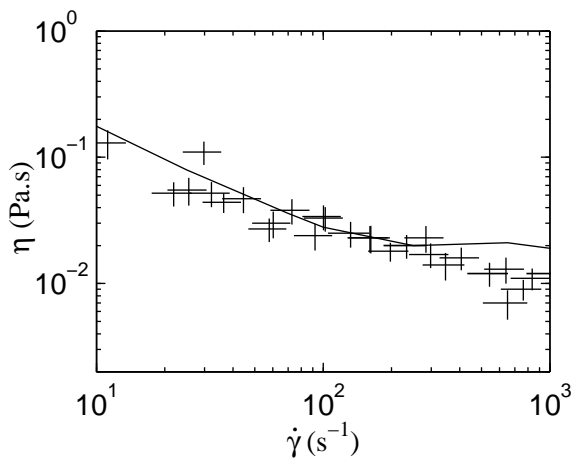


FIG. 17: Viscosity as a function of shear rate for the CTAB solution. + are results and error bars obtained with our microrheometer and line is the one obtained with a cone plate rheometer.

Figure 17 presents the flow curve obtained for the CTAB solution. The measurements are performed at 22°C. The values found with the microrheometer (see +) are in good agreement with the measurements performed on a classical cone plate rheometer (see line). There is a little deviation at high shear rates, where the CTAB

solution exhibits a shear thickening behavior. This thickening does not appear in our data. This may be due to the fact that the flow in our microchannel is not a pure shear flow as in a rheometer. During this experiment less than 300  $\mu\text{L}$  of fluid was injected into the system.

These data points out that we are able to identify the rheological nature of the fluid as well as its viscosity range at different shear rates with less than 350  $\mu\text{L}$  of sample in an automated fashion.

### Continuous formulation measurements

To benefit from the microfluidic approach and the low quantity of sample required to measure a flow curve, the formulations are prepared directly within the fluidic network. The concentration of the formulation is adjusted by defining appropriate flow rate ratio between the two miscible fluids in the initial flow rate file loaded at the beginning of the experiment. Figure 18 shows the results and error bars obtained for four mixtures of hexadecane and silicone oil at 100 mPa.s. The four mixtures are Newtonian fluids and the viscosity clearly increases when the fraction of silicone oil increases. The viscosity of the same mixtures prepared in vials are measured on a cone and plate rheometer (see lines on Fig. 18). Results are in quite good agreement. During this experiment only 1 mL of silicone oil and 1.2 mL of hexadecane was used.

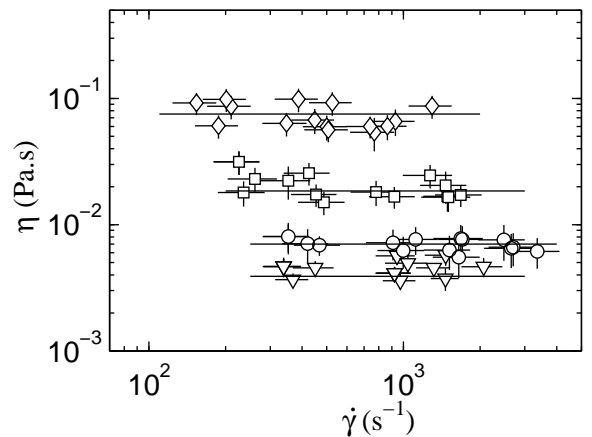


FIG. 18: Viscosity as a function of shear rate for four mixtures of hexadecane and silicone oil at 100 mPa.s.  $\nabla$  is a mixture obtained with a flow rate ratio between hexadecane and silicone oil ( $Q_{hd}/Q_{si}$ ) of 10,  $\circ$  with  $Q_{hd}/Q_{si}=4$ ,  $\square$  with  $Q_{hd}/Q_{si}=1$  and  $\diamond$  with  $Q_{hd}/Q_{si}=0.1$ . Lines are results obtained with a cone plate rheometer. Crosses behind symbols correspond to the calculated error bars on the shear rate and the viscosity.

Figure 19 presents the measurements performed for four formulations prepared in our set up by mixing a solution of PEO at 4 wt % with water prior injection into

our microrheometer. The lines on Fig. 19 were rheological measurements made on the same solutions prepared in a vial. Only 1.3 mL of PEO at 4 wt % was injected to obtain the four flow curves with our set up. They are in good agreement with the measurements of the cone and plate rheometer.

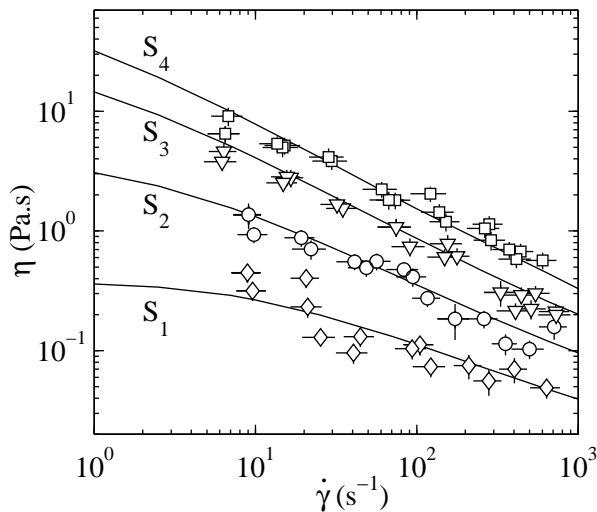


FIG. 19: Viscosity as a function of shear rate for four formulations of PEO in water. Lines are results obtained with a cone plate rheometer and symbols are results of the microrheometer.  $\diamond$  correspond to a solution  $S_1$  at 1 wt % of PEO,  $\circ$  to a solution  $S_2$  at 2 wt % of PEO,  $\nabla$  to a solution  $S_3$  at 3 wt % of PEO and  $\square$  to a solution  $S_4$  at 4 wt % of PEO. Crosses behind symbols correspond to the calculated error bars on the shear rate and the viscosity. During this experiment 1.3 mL of PEO at 4 wt % was injected.

Wormlike micelles solutions are not so easy to prepare in the fluidic network and the use of the IMM mixer is not efficient enough to obtain a homogenous solution at the outlet of the mixing device. This prevents the use of the IMM mixer as the only mixing stage on our network. To enhance mixing, a mixing chamber between the IMM mixer and the microfluidic chip has been added as discussed previously. Results obtained after these two mixing stages are presented in Fig. 20. The lines are results obtained with a cone and plate rheometer and the symbols are our results. The results and error bars obtained are in quite good agreement with cone and plate measurements and allow to see the increase of the viscosity when the surfactant concentration is increased.

1.1 mL of CpCl-NaSal at 6 wt % in brine water was used to get the three flow curves of the Fig. 20. This case illustrates that a larger amount of liquid is required when the mixture is pre-formulating in two mixers instead of a single one. This is obviously due to an increase of the dead volume between the mixing stage and the characterization chip. Note that the cone and plate rheometer data are not plotted after  $200 \text{ s}^{-1}$  because a large amount

of solution is ejected from the rheometer cell for higher shear rates.

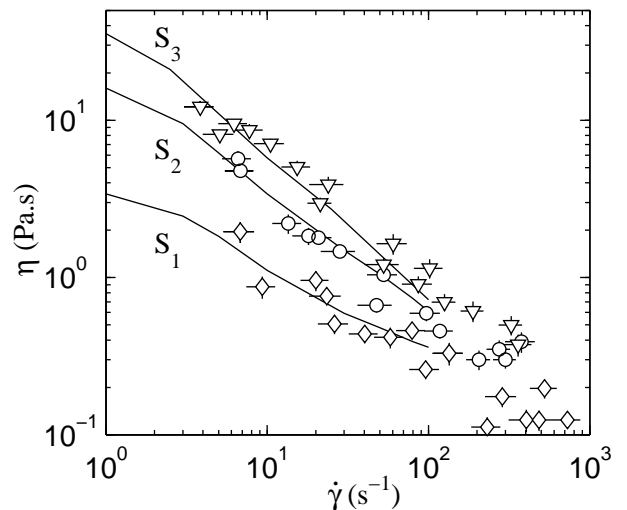


FIG. 20: Viscosity as a function of shear rate for three formulations of CpCl-NaSal at 6 wt % in brine water and water with 0.5 mol/L of NaCl. Lines are results obtained with a cone plate rheometer and symbols are results of the microrheometer.  $\diamond$  correspond to a solution  $S_1$  at 2 wt % of CpCl-NaSal,  $\circ$  to a solution  $S_2$  at 4 wt % of CpCl-NaSal and  $\nabla$  to a solution  $S_3$  at 6 wt % of CpCl-NaSal. Crosses behind symbols correspond to the calculated error bars on the shear rate and the viscosity. During this experiment 1.1 mL of CpCl-NaSal at 6 wt % in brine water was injected.

## Conclusions

In this work we described a method to perform automated rheological measurements on a microfluidic chip. We showed how to optically measure the rheological properties of complex fluids without the use of a transducer. Our method, which requires very few amount of sample, allows to get results that agree with classical macroscopic measurements with 10-20 % of error. By coupling this microrheometer with a mixing stage we engineered a fully automated set up which controls the sample concentration and the flow rates, analyzes the picture and calculates the mean shear rate and the viscosity to finally determine the flow curve. This is a first step towards obtaining a complete phase diagrams to select an appropriate formulation and make further studies on it. Mixing is clearly a key step for the screening of various formulations. This can limit our set up when a preparation requires very long time of equilibrium before being homogenous. But, in this case, no continuous measurement techniques are able to solve this problem. Nevertheless, our set up gives the behavior of the fluid under an applied stress and allows to estimate quite well its viscos-

ity range. Therefore it could be very useful in screening processes where the goal is to evaluate the flow curves of liquids and formulations in a continuous and fully automated way.

The authors gratefully acknowledge support from the Aquitaine Région. They wish to thank A. Ajdari and A. S. Utada for valuable discussions and D. Van Effenterre for his help during confocal microscopy experiments.

- 
- [1] P. Guillot, P. Panizza, J.-B. Salmon, M. Joanicot, A. Colin, C.-H. Bruneau, and T. Colin, *Langmuir* **22**, 6438 (2006).
- [2] R. G. Larson, *The Structure and the Rheology of Complex Fluids* (Oxford University Press, Oxford, 1999).
- [3] T. M. Squires, and S. R. Quake, *Review of Modern Physics* **77**, 977 (2005).
- [4] J. R. Van Wazer, J. W. Lyons, K. Y. Kim, and R. E. Colwell, *Viscosity and flow measurement* (John Wiley, New York, 1963).
- [5] J. S. Smith, N. M. N. H. Irving, and R. B. Simpson, *The Analyst* **95**, 743 (1970).
- [6] R. B. Simpson, J. S. Smith, and N. M. N. H. Irving, *The Analyst* **96**, 550 (1971).
- [7] P. W. Springer, R. S. Brodkey, and R. E. Lynn, *Polym. Eng. Sci.* **15**, 583 (1975).
- [8] D. J. Huskins, *Qualify Measuring Instruments in On-Line Process Analysis* (John Wiley, New York, 1982).
- [9] J. M. Dealy, *Chem. Eng.* **91**, 62 (1984).
- [10] Z. H. Silber-Li, Y. P. Tan, and P. F. Weng, *Experiments in Fluids* **36**, 586 (2004).
- [11] K. Kang, L. J. Lee, and K. W. Koelling, *Experiments in Fluids* **38**, 222 (2005).
- [12] J. M. Dealy, and A. Rey, *J. Non-Newtonian Fluid Mech.* **62**, 225 (1996).
- [13] P. Galambos, and F. Forster, *Intl. Mech. Eng. Cong. Exp.*, Anaheim, CA (1998).
- [14] A. Groisman, M. Enzelberg, and S. R. Quake, *Science* **300** **9**, 955 (2003).
- [15] A. Groisman, and S. R. Quake, *Phys. Rev. Lett.* **92**, 094501 (2004).
- [16] D. C. Duffy, J. C. McDonald, O. J. A. Schueller and G. M. Whitesides, *Anal. Chem.* **70**, 4974 (1998).
- [17] T. Thorsen, R. W. Roberts, F. H. Arnold and S. R. Quake, *Phys. Rev. Lett.* **86**, 4163 (2001).
- [18] J. D. Tice, A. D. Lyon, and R. Ismagilov, *Anal. Chim. Acta.* **507**, 73 (2004).
- [19] P. Guillot, and A. Colin, *Phys. Rev. E* **72**, 066301 (2005).
- [20] P. Guillot, A. Colin, A. S. Utada, and A. Ajdari, *Phys. Rev. Lett.* **99**, 104502 (2007).
- [21] R. F. Ismagilov, A. D. Stroock, P. J. A. Kenis, G. Whitesides, and H. A. Stone, *Appl. Phys. Lett.* **76**, 2376 (2000).
- [22] D. Huh, Y.-C. Tung, H.-H. Wei, J. B. Grotberg, S. J. Skerlos, K. Kurabayashi, and S. Takayama, *Biomedical Microdevices* **4**, 141 (2002).
- [23] E. Guyon, J.-P. Hulin, L. Petit, and C. D. Matescu, *Physical Hydrodynamics* (Oxford University Press, 2001).
- [24] R. B. Bird, W. E. Stewart, and E. N. Lightfoot, *Transport Phenomena* (Wiley, 2002).
- [25] R. Eymard, T. Gallouët, and R. Herbin, *Finite Volume Methods Handbook of Numerical Analysis* (P.G. Ciarlet and J.L. Lions, 2000).
- [26] *PHD 22/2000 Syringe Pump Series User's Manual* (Harvard Apparatus).
- [27] V. C. Hough, *Method and Means for Recognizing Complex Patterns* U.S. Patent No. 3,069,654 (1962).
- [28] P. E. Hart, and R. O. Duda, *Comm. ACM* **15**, 199 (1972).
- [29] W. Ehrfeld, K. Golbig, V. Hessel, H. Löwe, and T. Richter, *Ind. Eng. Chem. Res.* **38**, 1075 (1999).
- [30] T. Wu, Y. Mei, J. T. Cabral, C. Xu, and K. L. Beers, *J. Am. Chem. Soc.* **126**, 9880 (2004).
- [31] J.-F. Berret, D. C. Roux, and G. Porte, *J. Phys. II* **4**, 1261 (1994).
- [32] J.-F. Berret, G. Porte, and J.-P. Decruppe, *Phys. Rev. E* **55**, 1668 (1997).